RSC Advances

REVIEW

Cite this: *RSC Adv.*, 2015, **5**, 54793

Metal oxides and metal salt nanostructures for hydrogen sulfide sensing: mechanism and sensing performance

Zhi Guo,[ab] Guiqiu Chen,*[ab] Guangming Zeng,*[ab] Lingzhi Liu[ab] and Chang Zhang[ab]

Received 2nd June 2015
Accepted 17th June 2015

DOI: 10.1039/c5ra10394k

www.rsc.org/advances

This review presents a comprehensive summary of the development of strategies for H_2S recognition, which utilizes metal oxides (including CuO, SnO_2, ZnO, Fe_2O_3, WO_3, In_2O_3, BeO, NiO, and heterojunction) and metal salt nanostructures (including $Fe_2(MoO_4)_3$ nanorods and β-$AgVO_3$ nanowires) as the sensing materials. These sensors are based primarily on a conductivity response to H_2S. The sensing mechanism and performance of these systems are described in this review, and prospective development of sensors employing optical signals based on these materials is presented. In addition, the barriers and challenges in developing this system are also proposed. It is anticipated that excellent stability, high sensitivity, and easy detection under extreme conditions can be achieved with these systems.

1. Introduction

Hydrogen sulfide (H_2S) is one of the most toxic and odorous gases. It arises mainly from the decomposition of organic compounds and is also an industrial by-product.[1–3] The presence of H_2S in a system can lead to catalyst deactivation, environmental pollution, and especially pipeline corrosion.[4–7] H_2S-induced corrosion may cause energy and efficiency losses and structural failures resulting from the corrosion of pipes and equipment. Hence, an effective strategy for sensing H_2S is required as a measure for hazard prevention and control.

In the past few decades, H_2S sensors based on fluorescence imaging or colorimetric sensing have been extensively exploited in biological systems.[8–13] However, insufficient attention has been placed on H_2S sensing in nonbiological systems, in which H_2S gas is often present under high-temperature conditions and may enter the environment from the combustion of raw fuel, or from sewers and mines. Thus, sensors with enhanced properties are required to detect H_2S in nonbiological systems.[14–16]

Metal oxide semiconductors and metal salt nanostructures have recently been utilized as materials in gas sensing (including H_2S sensing) because of their availability, high-temperature stability, and easy fabrication.[17–22] H_2S gas sensors based on these species exhibit excellent sensitivity and catalytic properties under air atmosphere. To further enhance the response to H_2S gas even at a high working temperature,

[a]*College of Environmental Science and Engineering, Hunan University, Changsha 410082, P.R. China. E-mail: gqchen@hnu.edu.cn; Fax: +86 731 88823701; Tel: +86 731 88822829*

[b]*Key Laboratory of Environmental Biology and Pollution Control (Hunan University), Ministry of Education, Changsha 410082, P.R. China. E-mail: zgming@hnu.edu.cn*

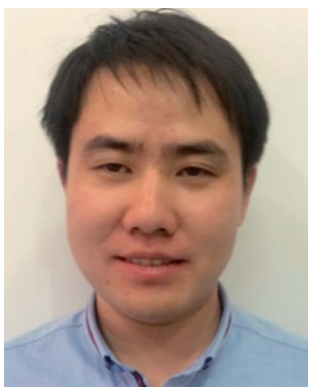

Zhi Guo received his bachelor's degree in environmental sciences from Anhui Normal University in 2012. He received his master degree from Hunan University. Now, he is pursuing a PhD degree in analytical chemistry and biosensor aspects at Hunan University. His research interests include chemical/biological sensors and portable sensing platforms, especially with novel detection systems.

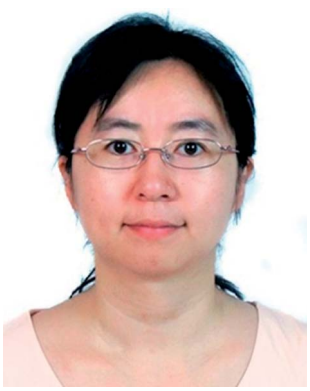

Guiqiu Chen received her PhD degree at Hunan University in 2006. She has worked as a chemical postdoctoral at Hunan University. She is a professor and doctoral supervisor in Hunan University now. Her research interests are nanosensor fabrication, fluorescence recognition of pollutants, bioimaging and also water pollution control.

scientists have proposed several techniques such as catalyst functionalization, element doping, and heterostructure formation in the fabrication of H_2S semiconductors.[23–27] The surface-depletion model has primarily been employed in the sensing mechanism.

In this review, we summarize recently developed H_2S sensors based on nanostructures, including metal oxide (CuO, SnO_2, ZnO, Fe_2O_3, WO_3, In_2O_3, BeO, NiO, and heterojunction) and metal salt nanostructures ($Fe_2(MoO_4)_3$ nanorods and β-$AgVO_3$ nanowire) that employ conductivity. The sensing mechanism and performance characteristics are presented and discussed. Moreover, future developments and challenges employing optical signaling based on these materials are proposed, and it is anticipated that excellent stability, high sensitivity, and ease of detection can be achieved with these systems under extreme conditions.

2. How the metal oxide semiconductors and metal salt nanostructures capable of H_2S recognition

In the past, many quantum dot, metal nanoparticles and organic dyes have been utilized in the gas detection including the reducing gas H_2S.[28–36] These sensors are mostly based on the optical properties of the materials as a sensing signal. The optical signal undoubted provides sensitive and naked eye approach to the gas recognition. However, H_2S is a gas often existed in extreme conditions[37–39] so that special attention should be given: are these sensors possess enough stability in these conditions? Would the signal be not disturbed by the environment? Was the signal easily enough to obtained under any conditions?

Generally, the organic dyes are easily to react with other matters that containing –SH, –COOH, and $–NH_2$ groups.[40,41] The quantum dot and metal nanoparticles have also been demonstrated to release metal ions and destroyed its special structures in the present of some materials or conditions variation.[42,43] The optical signal would be affected by many factors including the penetration and resonance properties of surroundings. These drawbacks have limited the potential applications of the quantum dot, metal nanoparticles, and organic dyes in H_2S detection.

As a sensor based on electron transfer between the gas molecule and the sensing material, metal oxide semiconductors and metal salt have been regarded as an excellent candidate for H_2S recognition due to their availability, high-temperature stability, and easy fabrication. As shown in Fig. 1, H_2S could selectively react with the surface matters such as adsorbed oxygen species to promote electron transfer, which induced conductivity changes of the sensor. Comparing to other sensors, metal oxide semiconductors and metal salt exhibited more stability in high temperatures; this promoted its application pipe, mine and so forth. In addition, the sensors were selective reaction with H_2S rapidly and the air exposure would absolutely recover its sensing ability in a short time. These characteristics indicate the prominent advantages in the application for H_2S detection.

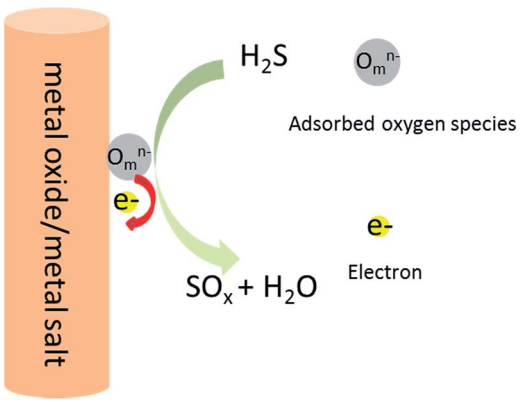

Fig. 1 Schematic illustration for H_2S sensing.

Guangming Zeng received his PhD from Wuhan University in 1988. Later, he worked at the College of Environmental Science and Engineering, Hunan University. Now he is a professor at Hunan University and also the director of Environmental Science and Engineering. His research interests include biosensor and bioimaging, especially fluorescence imaging in biological system based on QDs. After years of effort, he has been rewarded with many prizes and has cultivated hundreds of master degree candidates and doctoral candidates.

Lingzhi Liu received her bachelor's degree in environmental science from Jishou University. She has also achieved her master's degree at Hunan University. Her research interests include chemical/biological sensors and pollutant recognition. Her current research interests are gas recognition techniques, especially the toxic gases in sewage.

3. Metal oxide nanostructures for H_2S sensing based on conductivity

3.1. CuO nanostructures for H_2S sensing

CuO nanowire arrays have been fabricated for the detection of air-diluted H_2S at the parts per billion level.[44] When a low concentration of H_2S was introduced onto the CuO nanowires, H_2S reacted with the oxygen adatoms (O^-, O^{2-}, or O_2^-), and electrons released from the surface states recombine with the holes in the valence band maximum:

$$2H_2S(g) + 3O_2^{x-}(ad) \leftrightarrow 2SO_2(g) + 2H_2O(g) + 3xe^- \quad (1)$$

This induced a change in the conductivity of the sensors. However, a higher concentration of H_2S resulted in the surface reaction of CuO with H_2S to form a layer of CuS, covering the surface of the CuO nanowires:

$$CuO(s) + H_2S(g) \rightarrow CuS(s) + H_2O(g) \quad (2)$$

The formation of CuS caused a significant increase in the conductivity of the sensor. Based on this H_2S sensing mechanism, H_2S can be detected at concentrations as low as 500 ppb.

The CuO nanowire is one of the few metal oxide nanostructures that present p-type semiconducting properties. These nanowires have been shown to be very promising materials for chemical detection, especially for selective detection, if properly integrated with n-type nanowires. In addition, CuO is widely used in thin-film-based H_2S sensors such as the SnO_2 nanosensor described below.

3.2. SnO_2 nanostructures based sensors for H_2S

SnO_2 materials are the most widely utilized and studied semiconductor species for H_2S sensing due to the high surface-to-volume ratio, long life, and good sensitivity of these materials. SnO_2 is conventionally prepared by sol–gel,[45–47] sputtering,[48–50] evaporation,[51,52] chemical vapor deposition,[53–55] and plasma enhanced chemical vapor deposition methods.[56,57] The sol–gel method is the most commonly used technique, and the SnO_2 sol–gel nanocomposite product has been regarded as an excellent sensor material. The conventional sol–gel method is based on thermal agglomeration of SnO_2 nanopowder.[58]

Usually, excess hydrogen peroxide is first added to a solution of tin(II) acetate in glacial acetic acid:

$$Sn(CH_3COO)_2 + H_2O_2 + 2CH_3COOH \rightarrow Sn(CH_3COO)_4 + 2H_2 \quad (3)$$

Subsequently, a small amount of ammonia is added to the solution, leading to the formation of α-tin acid sol:

$$Sn(CH_3COO)_4 + 4NH_3 + 3H_3O \rightarrow H_2SnO_3\downarrow + 4CH_3COONH_4 \quad (4)$$

Finally, the α-tin acid sol is precipitated by centrifugation. SnO_2 nanopowder is then obtained *via* calcination of the α-tin acid sol:

$$H_2SnO_3 \rightarrow SnO_2 + H_2O \quad (5)$$

The obtained SnO_2 nanopowder is mixed with glycol to achieve the SnO_2 sol–gel. SnO_2 sol–gel nanomaterials obtained by this method exhibited uniform size distribution, high purity, small particle size, and excellent activity.[59]

The surface-to-volume ratio and surface electrical conductivity are generally regarded as the main factors for improving the sensitivity of the sensors.[60,61] In this regard, one-dimensional metal oxide SnO_2 nanowires and thin films with high surface-to-volume ratio, especially those doped with metals or metal oxides, have recently emerged as an alternative to SnO_2 sol–gel nanocomposites for H_2S gas sensing. Sun *et al.* demonstrated that well-ordered porous Cu-doped SnO_2 thin films have greater sensitivity and a shorter response and recovery time than the undoped porous SnO_2 thin film sensors (Fig. 2).[62] The thin film was prepared by simple sputtering deposition using a self-assembly film of polystyrene spheres as a soft template. Due to the controllable pore size and the homogeneity of the film thickness, the sensing performance was well regulated. Sun *et al.* also proposed that the Cu-doped SnO_2 thin films operate by a mechanism that is commonly observed for Cu- and CuO-doped SnO_2 semiconductors:

The Cu dopant in the film exists in the form of CuO crystalline grains. When the sensor is exposed to H_2S, CuO is converted to CuS as confirmed by Tang *et al.* in 2010.[63] Because of the good electrical conductivity, the electronic interaction between CuO and SnO_2 that gives rise to a very large electrical resistance of the sensor is disrupted upon exposure to H_2S, leading to a drastic decrease in the electrical resistance and hence to the extremely high H_2S sensitivity. When air is introduced and H_2S is removed from the sensor, CuS is immediately reconverted to CuO (Fig. 3).

$$CuS(s) + \frac{3}{2}O(g) \rightarrow CuO(s) + SO_2(g) \quad (6)$$

Because of this reaction, the electronic interaction between CuO and SnO_2 is restored with concomitant recovery of the original electrical resistance.

Dai *et al.* evaluated the mechanism of adsorption of H_2S and O_2 on the SnO_2 (110) surface in the absence and presence of doped Cu, as well as the effect of Cu doping on SnO_2 selectivity,

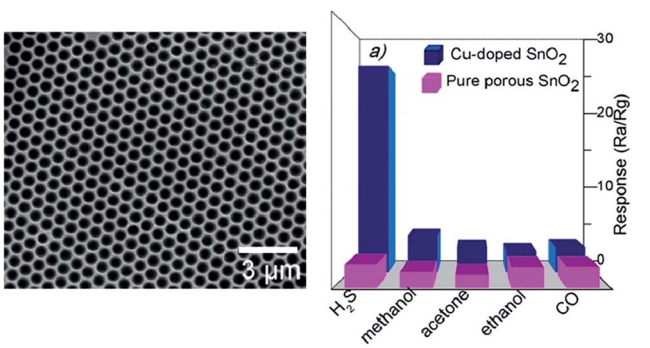

Fig. 2 SEM of porous Cu-doped SnO_2 sensor and its selectivity.[62]

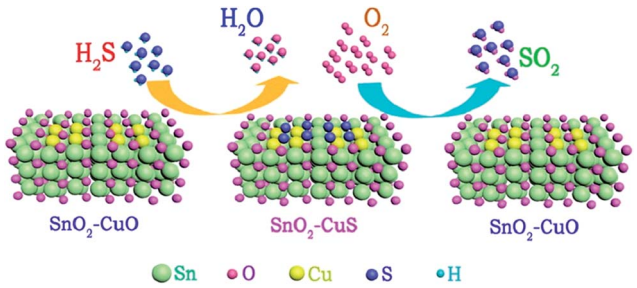

Fig. 3 Proposed sensing mechanism of Cu and CuO doped SnO_2 sensor for H_2S gas.[62]

by means of first-principles calculations based on the density functional theory.[64] As shown in Fig. 4, H_2S is dissociatively adsorbed on the SnO_2 (110) surface with one H atom converged to a bridging oxygen atom, while the HS complex is bonded to a pentacoordinate Sn atom. H_2S adsorption does not change the electronic structure of the (110) surface and H_2S does not inject electrons into the band-gap, indicating that H_2S has little effect on the electrical conductivity of the nondoped SnO_2 (110) surface. In the case of Cu-doped SnO_2, electrons from the H_2S states are injected into the band-gap and into the conduction band during the adsorption process. Thus, charge transfer from the molecule to the semiconductor occurs. The electrical conductivity of SnO_2 is thereby improved, and Cu-doped SnO_2 exhibits sensitivity toward H_2S gas. Furthermore, Cu doping promotes the formation of oxygen vacancies on the SnO_2 surface, thus increasing the surface potential barrier and electrical resistance. When H_2S is present, there is a more pronounced decrease in the electrical resistance, which may be another reason for the high sensitivity of the Cu-doped SnO_2.

In addition to Cu and CuO-doped SnO_2 sensors, many other metal or metal oxides such as Fe, Pd, Ag, and Pt have also been used to improve the sensing properties of SnO_2. For example, an Fe-doped SnO_2 film exhibited highly selective sensing behavior toward H_2S even at room and high temperatures. The sensor showed around 45% response at room temperature even for 10 ppm H_2S in a short response and recovery time, which further increased as the gas concentration and operating temperature increased.[65] The porous, 16 nm-thick, Ag-doped SnO_2 film exhibited improved sensitivity toward H_2S relative to the SnO_2 film. Upon addition of H_2S, the as-deposited Ag film was transformed to Ag_2S, which enhanced the sensitivity of the sensor at 200 °C.[66]

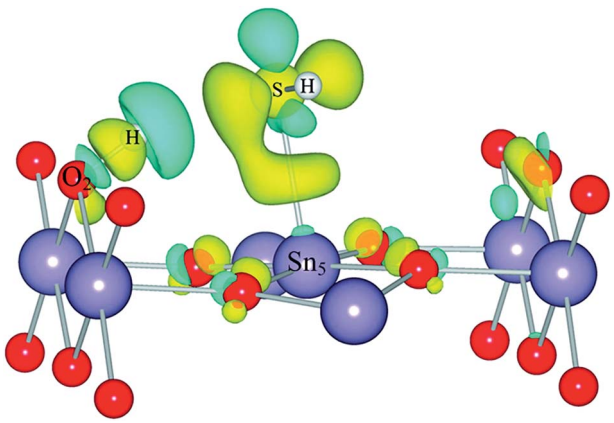

Fig. 4 Charge density difference for H_2S adsorption on the stoichiometric SnO_2 (110) surface. The cyan region represents charge depletion and the yellow region represents charge accumulation.[64]

Metal or metal-oxide doping significantly improved the sensing sensitivity, response, and recovery time of the SnO_2 sensors. This opens up the possibility for exploring the effect of dopants on the SnO_2 nanostructures to achieve excellent H_2S gas sensing.

3.3. ZnO nanostructures based sensors for H_2S

ZnO, a wide band-gap material (3.37 eV) with a wurzite crystal structure, has been studied as a H_2S sensing material with good sensing properties, including speedy response and recovery. The surface-depletion model is generally used to describe the sensing mechanism. During the sensing process, H_2S can interact with the surface or be directly adsorbed on the oxide surface, or interact with preadsorbed oxygen present on the surface. When the gas is adsorbed, the thickness of the depletion layer may be altered, inducing a change in the measured resistivity.[67] Ghimbeu *et al.* demonstrated the surface reaction of H_2S with adsorbed oxygen species, similar to the surface reaction of CuO nanowires.[68] The reaction with H_2S induced changes in the thickness of the depletion layer, which may stimulate a resistance-type sensing signal.

Chemical conversion of ZnO is regarded as another possible reaction route for H_2S sensing. Yong *et al.* demonstrated the formation of Zn–S bonds in ZnO nanosensors, which becomes a dominant sensing mechanism at temperatures above 300 °C.[69] As shown in Fig. 5, the oxygen species were initially adsorbed onto the ZnO surface, forming a rather thick depletion region (Fig. 5A). Exposure to H_2S promoted the surface reaction with the adsorbed oxygen species, which thinned the depletion layer and increased the conductivity (Fig. 5B). However, the decomposition of H_2S in ZnO to form Zn–S bonds was regarded as the main sensing mechanism when the temperature was higher than 300 °C (Fig. 5C). This reaction caused the formation of a shallow donor level and induced a drastic increase in the conductivity of the sensor.

To further investigate the specific surface reaction after the adsorption of H_2S, Spencer *et al.* examined the gas-surface reaction by employing three different one-dimensional (1-D) ZnO nanostructures, a hexagonal nanowire, a faceted-nanotube, and a zigzag (9,0) nanotube, using density functional theory calculations.[67] A clean ZnO surface was required for interaction with H_2S. The results showed that H_2S molecules were physisorbed on the nanotube. However, the molecules were dissociated into H and SH after adsorption on the nanowire and faceted-nanotube. H_2S behaves as a charge donor, where the charge is transferred from H_2S to the nanostructure. When H_2S interacts with the nanostructure surface, the band-gap of the nanowire and faceted-nanotube decreases greatly, while that of the nanotube changes only slightly.

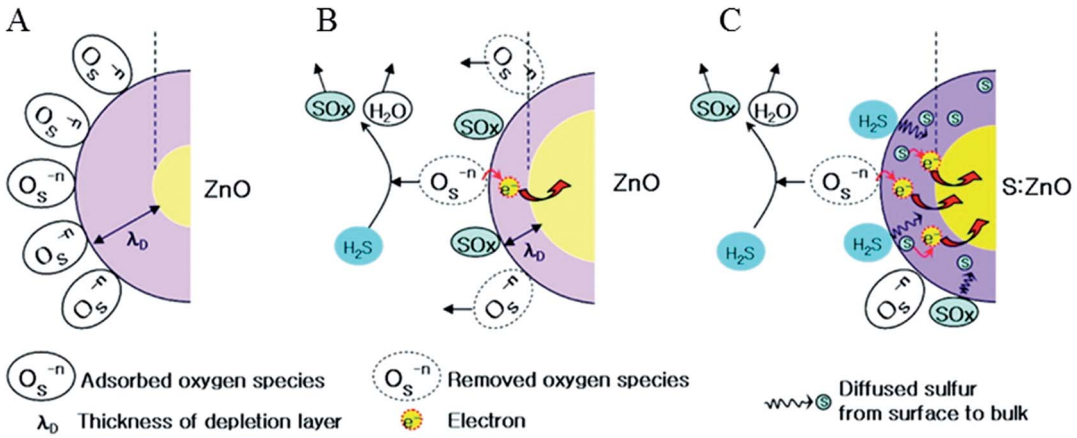

Fig. 5 Schematic of H_2S sensing with ZnO nanosensor (A) oxygen ionosorption surface before sensing, (B) H_2S gas adsorption and surface reaction with surface oxygen and (C) donor level formation of ZnO with sulfur chemisorption at temperature above 300 °C.[69]

Many ZnO-based sensors have been fabricated for H_2S detection with good performance. ZnO nanorods synthesized by the hydrothermal method exhibited a strong response and good selectivity to low concentrations of H_2S (0.05 ppm) at room temperature.[70] ZnO nanorods synthesized by a solid-state technique were demonstrated to be selective for H_2S at the relatively low working temperature of 190 °C.[71] The response and recovery times of as-prepared ZnO were less than 5 s and 16 s, respectively. Srivastava *et al.* demonstrated that modification of ZnO with sensitizers could enhance the sensing performance to some extent, especially for $Au_{5.7at\%}$-modified ZnO nanowires with response and recovery times of 22 s and 52 min, respectively.[72] The maximum sensor response of 52 was obtained at the optimal temperature of 300 °C for H_2S. These sensors are versatile platforms for potential fabrication of more suitable H_2S sensing devices.

3.4. Fe_2O_3 nanostructures based sensors for H_2S

α-Fe_2O_3, the most stable iron oxide usually with n-type semiconducting properties (E_g = 2.1 eV) under ambient condition, has been widely used as gas sensors.[73–77] It shows the most fascinating properties that it undergoes both "n to p" as well as "p to n" transitions (Fig. 6).[78] As shown in Fig. 6, O^- or O^{2-} are dominated forms instead of O_2^- at high temperatures (350 °C or even higher), which capture more electrons from the conduction band. As a result, the conductivity nature of the sensor performed a change from n-type p-type transition.

Usually, it has a complex defect structure with three types of defect species *i.e.* oxygen vacancies, Fe^{3+} interstitials and Fe^{2+} interstitials.[79,80] Singh *et al.* have investigated the sensing properties of pure nano-crystalline Fe_2O_3 films towards H_2S.[79] The assays indicated that Fe_2O_3 films prepared by electron-beam evaporation of Fe exhibits n-type conductivity. The

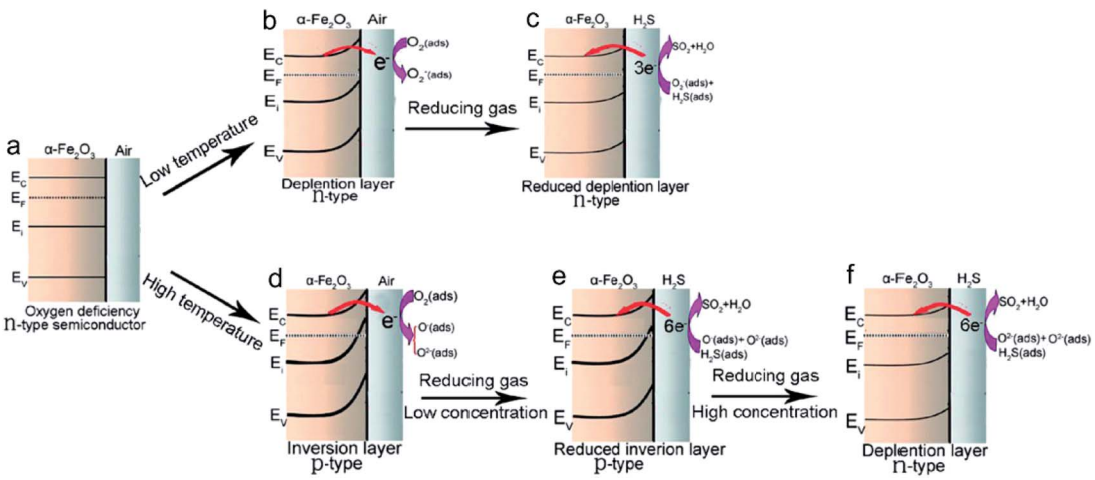

Fig. 6 Schematic energy–level diagrams of: (a) an n-type semiconductor caused by oxygen vacancies; (b) an n-type semiconductor with depletion layer caused by mild surface absorption; (c) an n-type semiconductor with reduced depletion layer caused by surface reaction with reducing gas; (d) a p-type semiconductor through formation of an inversion layer caused by strong surface absorption due to the large density of surface defect states; (e) a p-type semiconductor with reduced inversion layer caused by surface reaction with low concentrations of reducing gas; (f) an n-type semiconductor with depletion layer caused by surface reaction with high concentrations of reducing gas.[78]

resistance change of α-Fe_2O_3 was regarded as dependence on the species and chemisorbed oxygen (O_2^-, O^{2-} and O^-) on the surface according to the classical electron depletion theory.[81,82] Oxygen absorption would cause the electron depletion, and consequently the resistance of the sensor changes. Upon H_2S is exposed, it is oxidized by these chemisorbed oxygen species on the surface of the sensor. Then, the electrons move back into the semiconductor, resulting in a reverse change in resistance of the sensor. At the operating temperature of 250 °C, atmospheric oxygen is adsorbed in O^- form, results in capture of electrons from conduction band and trapping them at the surface. This reaction further leads to a decrease in conductance of the films. After exposure of 50 ppm H_2S, the captured electrons are released back to the conduction band. The conductance of the sensor will increase within 64 s simultaneously.

α-Fe_2O_3 nanochains have been successfully fabricated *via* an ammonium acetate-based ionothermal synthetic route for H_2S with the lowest concentration of 3 ppm.[83] With the temperature increasing from 270 to 345 °C, the sensitivity of the sensor decreases gradually. However, the recovery time varied from 160 s at 270 °C to 15 s at 345 °C with increasing working temperature. It exhibited an optimized performance temperature at 285 °C. Microwave-assisted hydrothermal method coupled with an annealing technique was used to fabricate porous α-Fe_2O_3 nanospheres and nanorods that were demonstrated superior to the α-Fe_2O_3 nanochains described above.[84] As shown in Fig. 7, the nanospheres and nanorods showed excellent sensitivity to H_2S comparing to commercial α-Fe_2O_3 sensor. The sensitivity towards H_2S has also demonstrated much higher than to other gases.

Pd-doped α-Fe_2O_3 has been synthesized by Wu *et al.*[85] This sensor exhibited higher response, better selectivity, and faster response and recovery to H_2S compared to the pure α-Fe_2O_3. Interestingly, the Pb doping decrease the performance temperature, which is a progress to energy saving. The assays indicated that 1.5 wt% doping produce the largest response of 128.3 to 100 ppm H_2S at 160 °C. The same groups also fabricated Pt-doped α-Fe_2O_3 thick film for H_2S.[86] The as-synthesized sensor also exhibited excellent advantages in comparison of undoped α-Fe_2O_3 sensor. 2 wt% Pt doped α-Fe_2O_3 showed the best response towards 10 ppm H_2S.

By doping the α-Fe_2O_3 nanoparticles with 5 nm spherical Ag grains, Wu *et al.* developed a low temperature H_2S sensor.[87] Ag doping enhanced surface area of the sensor, with the benefits to better sensing performance including response, selectivity, and optimum operating temperature. Similarly to the Pt doped α-Fe_2O_3 reported above, addition of 2 wt% Ag and calcined at 400 °C exhibited the maximum response to H_2S at 160 °C. The doping technology has been regarded as an effective method in promoting the sensing performance of the pure α-Fe_2O_3 nanomaterials.

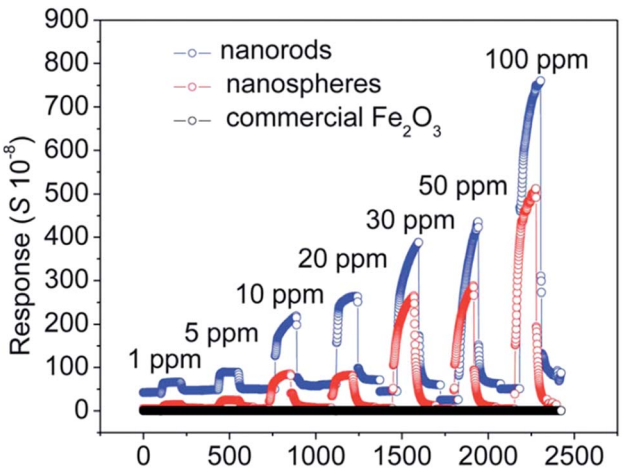

Fig. 7 The response curve of the α-Fe_2O_3 based sensor to H_2S gas with increasing concentration at a working temperature of 350 °C.[84]

3.5. WO_3 nanostructures based sensors for H_2S

WO_3 nanosensors with hexagonal and monoclinic morphology were produced for selective recognition of H_2S.[88] Monoclinic WO_3 responded to all five evaluated gases (CH_4, CO, H_2, NO, and H_2S) at 200 °C. However, the gas sensing signal for 10 ppm H_2S was two orders of magnitude greater than that for the other gases, and the sensing process could be performed even at 25 °C. In contrast, hexagonal WO_3 was selective to H_2S only, and the response time for 10 ppm H_2S was significantly faster than that of monoclinic WO_3 despite the lower selectivity compared to monoclinic WO_3.

Ramgir *et al.* compared the effect of various Au loadings on H_2S sensing by WO_3.[89] The results showed that Au-incorporated WO_3 films exhibited better sensing performance than the pure WO_3 sensor films. Taking 0.7 ppm H_2S as an illustration, the pure WO_3 films exhibited a sensitivity of 2.9 with respective response and recovery times of 106 s and 32 min, while the Au-incorporated sample (2.32 at.%) exhibited an increase in the sensitivity to 12 with response and recovery times of 88 s and 18 min, respectively. The WO_3 sensor doped with 2.32 at.% of Au could detect H_2S with an enhanced sensitivity of about 16 at an operating temperature of 250 °C. This enhancement was mainly caused by the doping element Au that imparted sensitivity to WO_3 *via* the electronic sensitization mechanism.[90] The interaction with H_2S occurred primarily on the Au surface, and the corresponding changes were transferred immediately to the host matrix, reflected as a rapid decline in the resistance of the sensor. Doping was regarded as an effective method for improving the sensing performance of the sensor. In addition to Au, many other materials such as Pd nanoparticles have been successfully doped into WO_3 films, resulting into enhanced sensitivity to H_2S.[91]

3.6. In_2O_3, BeO, and NiO nanostructures based sensors for H_2S

In_2O_3-based materials have been fabricated for various gas sensing applications, including H_2S sensing, due to their advantageous features such as wide band-gap (around 3 eV) and low resistance.[92–94] In_2O_3-based materials possess ultra-high surface-to-volume ratios, and are expected to be superior gas sensor candidates and alternatives to thin-film sensors.

The H_2S-sensing performance of vanadium-doped In_2O_3 nanofibers fabricated by electrospinning was characterized at different temperatures ranging from 50 to 170 °C.[95] The sensor based on 6 mol% V-doped In_2O_3 nanofibers exhibited the highest response, *i.e.*, 13.9–50 ppm H_2S, at the relatively low temperature of 90 °C (Fig. 8). In addition, this sensor had a rapid response time of 15 s and recovery time of 18 s, and good selectivity.

BeO nanotubes (BeONT) have been successfully applied to H_2S sensing. In 2004, Ahmadaghaei *et al.* performed a detailed study of the specific sensing properties of BeONT using density functional calculations.[96] The results showed that gas molecules are physically adsorbed on pristine BeONT with adsorption energies ranging from 3.0 to 4.2 kcal mol^{-1}. Si doping induced the substitution of Be or O atom in BeONT by Si, thus increasing the adsorption energy to 6.9–17.2 kcal mol^{-1}. Notably, upon substitution of an O atom by Si, the electronic properties of BeO were altered with a dramatic increase in the energy gap from 2.78 to 3.93 eV after H_2S adsorption, making BeONT strongly sensitive to the H_2S molecule.

As a p-type material with band gap ranging from 3.6 to 4.0 eV, NiO is a very attractive sensing material applied in resistive type gas sensors.[97–100] NiO with Fe_2O_3 loading exhibited excellent sensitivity comparing to the pure NiO sensor (Fig. 9).[101] The sensor displayed p-type semiconductors characteristics due to extra-high molar ratio of NiO to Fe_2O_3. It is proposed that H_2S molecules were first adsorbed on the surface, providing electrons to the surface of NiO nanoplates. The adsorption increased the potential barrier and hence, enhanced the resistance of sensor.

3.7. Sensors for H_2S based on p–n, p–p, or n–n heterojunction

P–n heterojunction has attracted much attention in the fabrication of gas sensors recently.[102–104] Generally, the formation of heterojunction produces an electrical barrier between crystal grains,[105] which promoted the sensitivity to reducing gases.[106] Yong *et al.* have fabricated p–n heterojunction CuO/ZnO nanorods for H_2S recognition and exploited the special sensing mechanism.[107] As shown in Fig. 10a, metal oxide sensing materials showed high resistance due to the adsorption of oxygen species, resulting in a depleted region on the surface. When exposed to H_2S, the adsorbed oxygen species was removed by H_2S, with the subsequently generation of metallic Cu_2S due to reaction of CuO with H_2S as shown in Fig. 10b. This chemical conversion of CuO into metallic Cu_2S induced the change of energy band structure and increased the conductivity of the sensor. The response of CuO-doped ZnO to H_2S gas was identically enhanced compared to that of the bare ZnO nanorods due to chemical conversion of CuO into CuS upon exposure to H_2S, which destroyed the p/n junction of the sensor.[108]

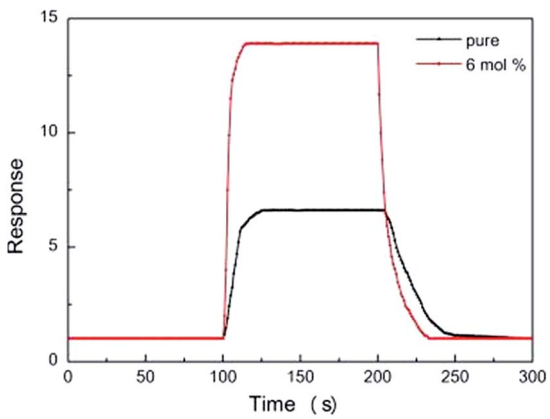

Fig. 8 The response and recovery characteristics of pure and 6 mol% V-doped In_2O_3 to 50 ppm H_2S at 85 °C and 90 °C respectively.[95]

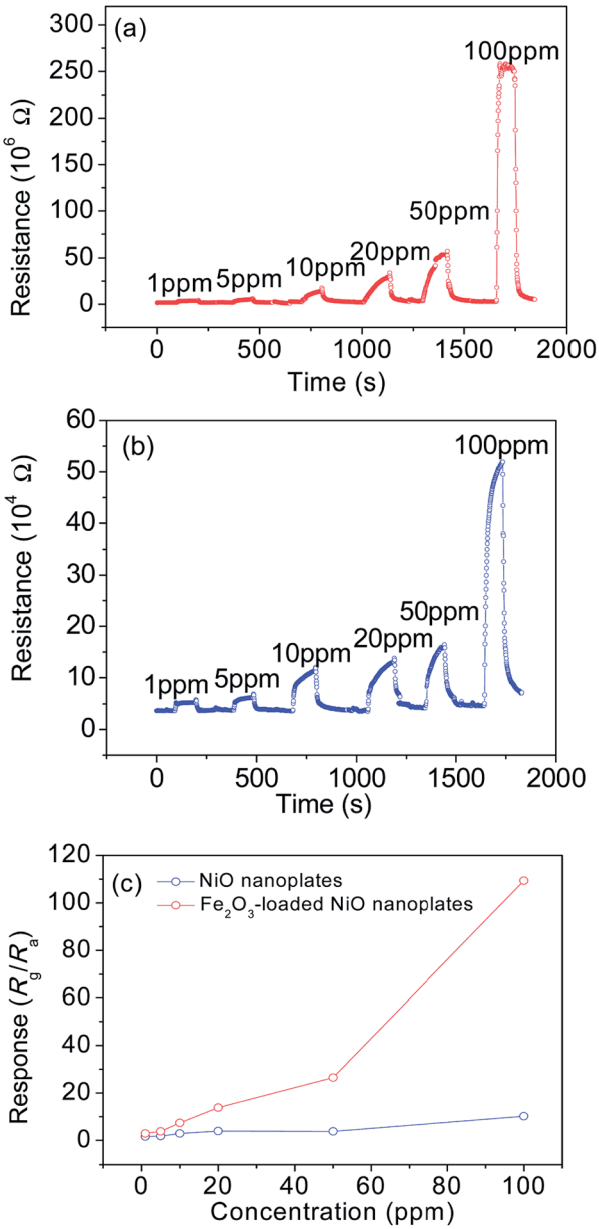

Fig. 9 Response curve of (a) NiO loaded with Fe_2O_3 nanoplate; (b) pure NiO nanoplate sensors to H_2S at a working temperature of 200 °C; (c) the relationship between the response and H_2S concentration.[101]

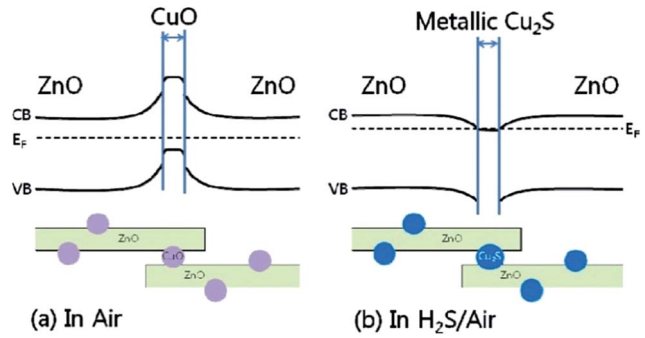

Fig. 10 Changes in energy band structures of the CuO/ZnO nanorods (a) before and (b) after exposed to H_2S.[107]

By combining the advantages of high accessibility of gas to the nanofibrous structures and the distinctive chemical interaction between CuO and H_2S, the gas response of pure In_2O_3 to H_2S was significantly enhanced *via* CuO loading.[109] The CuO-doped In_2O_3 nanofibers possessed high specific surface area and abundant p–n junctions due to uniform mixing between p-CuO and n-In_2O_3 nanograins within the nanofibers. Exposure to H_2S resulted in a change of the resistive heterojunction between p-type CuO and the n-type oxide semiconductor into a conductive junction between metallic CuS and the n-type oxide semiconductor, which provided an ultrasensitive and ultra-selective signal to H_2S based on conductivity changes. As shown in Fig. 11, the response of the CuO-loaded In_2O_3 nanofiber to H_2S at 25–450 °C was remarkably high. At 150 °C, the gas response (ratio of the resistance in air to that in gas) toward 5 ppm H_2S increased from 515 to 1.16×10^5.

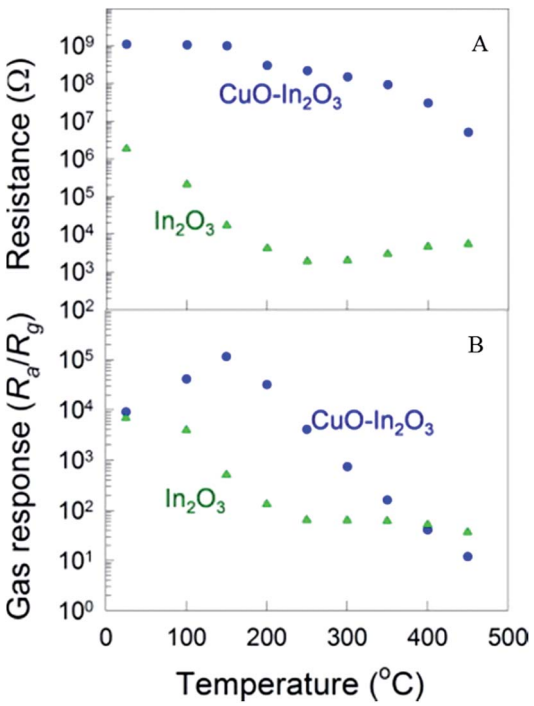

Fig. 11 (A) Sensor resistance in air (R_a) and (B) gas response (R_a/R_g) of pure and CuO-loaded In_2O_3 composite nanofibers at 25–450 °C.[109]

NiO doped with ZnO produced a p–n heterojunction that enhanced H_2S sensing properties.[110] Generally, the variation of nanostructure and surface activity of ZnO and NiO nanocrystals accounts for the enhancement of the sensing properties. The particular continuous nanostructure of both NiO and ZnO has suitable contacted area, which resulted in appropriate p–n junction formation and created strong interaction. In the presence of 50 ppm H_2S, the best structure of the sensor exhibited the fastest switching dynamics to H_2S at optimal temperature with average response time ~50 s and recovery time ~124 s. This response and recovery time is much lower than pure NiO sensor in the same sensing temperature.

The n-typed SnO_2 nanowires decorated by p-typed NiO nanoparticles exhibited up to ~351-fold response to 10 ppm H_2S at 300 °C with the value reaching to 1372.[111] However, the cross-gas responses to 5 ppm NH_3, 200 ppm C_2H_5OH, and 1 ppm NO_2 were 1.6, 2.1, 1.8 respectively, which indicating the excellent selectivity. In the past, many metal nanoparticles have been dispersed inside the sensors to enhance its performance. As one of the most attracted nanomaterial, Au nanoparticles have been demonstrated the best candidate additive to promote gas sensor characteristics.[112]

The p-typed CuO was covered with p-typed NiO to achieve CuO–NiO core–shell structure by Zhou *et al.*[113] Although it is a p–p heterojunction, the assembly obviously enhanced H_2S sensing properties, because of the catalytic effect of NiO and formation of heterojunction at the interface between CuO and NiO inducing electrons transfer from CuO to NiO to equalize the Fermi levels.

ZnO modified with additive TiO_2 could greatly improve the gas sensing properties of sensors. The ZnO : TiO_2 complex with 10 mol% CdO showed excellent electrical resistance response toward H_2S an operating temperature of 225 °C.[114] The sensitivity increased with an operating temperature up to 225 °C; and a further increase in temperature resulted in decreases of sensitivity.

4. Metal salt for H_2S sensing based on conductivity

Metal salts possess useful properties that help in gas sensing applications and hence they act as important functional materials.[115,116] Porous iron molybdate ($Fe_2(MoO_4)_3$) nanorods with an average diameter and length of 200 nm and 1.2–4 μm, respectively, have been used to detect H_2S gas at concentrations as low as 1 ppm at a relatively low working temperature of 80 °C (Fig. 12).[117] Moreover, the porous nanorods had fast response and recovery times, good selectivity, and long-term stability due to the small size effect, porous characteristics, and catalytic activity at low temperature. The good sensing performances of $Fe_2(MoO_4)_3$ nanorods was attributed two aspects: (1) many pores of the matter benefits the diffusion of more of H_2S gas molecules into the nanorods; (2) H_2S reacts with the adsorbed oxygen to release electrons and catalytic ability of the matter at low temperatures promoted the process. The released electrons will decrease the resistance of the nanorods, which accounts for the response to H_2S.

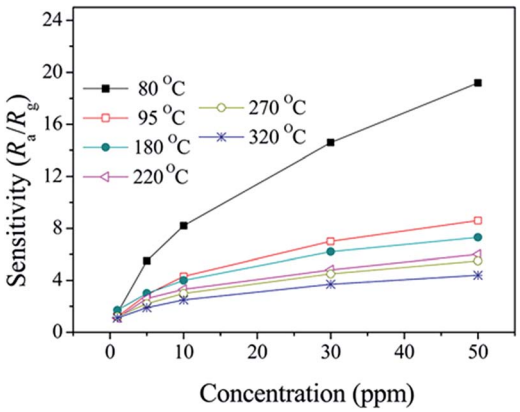

Fig. 12 Sensor responses of the porous $Fe_2(MoO_4)_3$ nanorods to H_2S gases with different concentrations at different working temperatures.[117]

Single β-$AgVO_3$ nanowire exhibited a "threshold switching" phenomenon that high bias (>6 V) will switch the individual nanowire device from nonconductive to conductive (Fig. 13).[118] After applying high bias of 6 V, nanoscale metallic Ag appeared that may be related to the electrical switching of β-$AgVO_3$ nanowire. The resistance of the sensor decreased quickly after exposure to H_2S and then gets saturated. However, the resistance increases and returns nearly to its baseline value when cutting off the H_2S supply. The reproducibility of the sensor will not be destroyed.

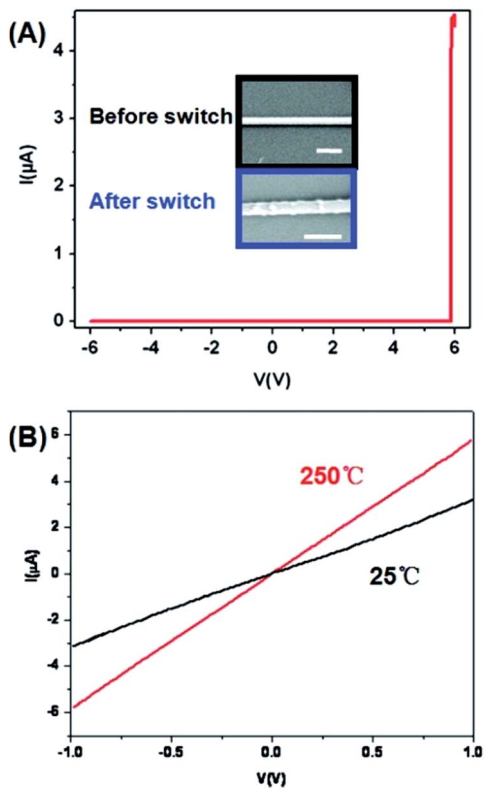

Fig. 13 *I*/*V* curves of β-$AgVO_3$ nanowire (A) at high bias of 6 V (inset showing SEM image of β-$AgVO_3$ nanowire before and after switch); (B) at the bias of 1 V after applying high bias of 6 V at 25 and 250 °C.[118]

Table 1 summarizes a range of sensors and shows a comparison of their best sensing performance parameters, *i.e.*, the concentration, temperature, response time, recovery time, and sensitivity. The sensitivity was estimated based on the percentage response, which is defined as:

$$\text{Response } (\%) = \frac{R_a - R_g}{R_a} \times 100 \quad (7)$$

where R_a is the resistance of the sensor in air and R_g is the resistance in the presence of a test gas.

5. Summary and perspective

H_2S is of particular interest because of its impact in metal corrosion and physiological equilibriums. Many semiconductor materials have therefore been developed to assess the levels of H_2S under different conditions. Metal oxide semiconductors and metal salt nanostructures are extremely attractive for H_2S sensing due to their rapid response, high selectivity, and stability. These materials are mainly based on (1) metal oxides, including CuO, SnO_2, ZnO, Fe_2O_3, WO_3, In_2O_3, BeO, NiO, and heterojunction; and (2) metal salt nanostructures, including $Fe_2(MoO_4)_3$ nanorods and β-$AgVO_3$ nanowire. Most of these sensors exhibit a conductivity response to H_2S. However, this sensing mechanism has some limitations as well, such as difficulty in detecting the signal and the sensitivity of the signal to the conditions, especially temperature changes.

As shown in Table 1, Fe_2O_3 nanosensors exhibit relatively higher sensitivity and a faster response comparing to other sensors. In general, the doped sensors have a fast response in a mild temperature not only high temperature that needed by the pure one. We cannot discover obvious advantages of metal salts compared to the metal oxides nanosensors. However, β-$AgVO_3$ nanowire showed a short response and recovery time for 50 ppm H_2S that should be noticed by the researchers.

Although the conductivity based sensors have many advantages, the sensitivity is much lower than optical sensors.[8] To apply the sensor in low H_2S surroundings, the sensitivity should be improved further. For example, the doped sensor could recognise H_2S at room temperature. The sensors with high sensitivity are competent for high temperature and biological system simultaneously. In addition, the conductivity signal is somewhat inconvenient to obtain.

Recently, optical sensors have been successfully employed to overcome these drawbacks, and H_2S optical sensing provides a signal that can be easily detected by the naked eye. However, the optical sensors primarily employ organic dyes, which may result in reduced stability under extreme conditions.[8] Metal oxides and metal salts exhibit excellent stability under harsh conditions, although few studies of optical sensors based on these materials have been reported. The development of optical sensors based on metal oxides and metal salts is therefore required for recognition of H_2S under extreme conditions. Notably, how to avoid the optical signal not to be interfered and be acquired completely are also important.

Table 1 Best sensing performance of the metal oxides and metal salt nanosensors

Type	Constitute/structure	Concentration (ppm)	Temperature (°C)	Response (%, $(R_a - R_g)/R_a$)	Response time (s)	Recovery time (s)	Dimension parameter	Matrix environment	Reference
CuO	CuO nanowire	0.5	160	[a]	[a]	~500	Dia. 80–200 nm, len. 4–8 μM	Thin copper plate	44
SnO_2	SnO_2 nanowire	1.4	400	29	76	203	Dia. 30–400 nm, len. 100 μM	Si wafer with SiO_2 layer	119
	SnO_2 thin film	1.4	300	91	39	336	Thi. ~50 nm	Si wafer with SiO_2 layer	119
	Cu-doped SnO_2 thin film	100	180	96	10.1	42.4	Thi. 100 nm	Si wafer with SiO_2 layer	62
	Fe-doped SnO_2 nanoparticle	50	20–25	99	5–10	95–105	Dia. 18 nm	Au patterned alumina substrate	65
	Ag-doped SnO_2 film	1	200	~100	[a]	[a]	Thi. 100 nm	Oxidized silicon substrate	66
ZnO	ZnO thin film	12	450	44	[a]	[a]	Dia. 17–21 nM	Alumina pellet	68
	ZnO nanorod	0.05	25	41	~1500	>450	Dia.70–110 nm, len. 0.2–1.3 μm	Al_2O_3 tube	70
	ZnO nanorod	100	190	97	5	16	Dia. 15–40 nm, len. 200 nm	[a]	71
	Au modified ZnO nanowire	10	300	98	22	3120	[a]	$Si/Si0_2$ substrates	72
Fe_2O_3	Porous urchin-like α-Fe_2O_3	1	250	[a]	5	10	Dia. 30–40 nm, len. 500 nm	Alumina tube	78
	Fe_2O_3 thin film	1	250	50–67	64	390	Thi. 100 ± 10 nm	Al_2O_3 substrate	79
	α-Fe_2O_3 nanochain	1	285	67–75	8.6	65.7	[a]	[a]	83
	Pd-doped α-Fe_2O_3 nanoparticle	100	160	99	[a]	~500	Dia. 30–50 nm	Alumina tube	85
	Porous α-Fe_2O_3 nanosphere	1	350	70.6	[a]	4.1	Dia.50 nm	[a]	84
	Pt-doped α-Fe_2O_3 thick film	10	160	99	[a]	~700	Thi. 50 μm	Alumina tube	86
	Ag-doped α-Fe_2O_3 nanoparticle	50	160	98.6	68	35	Dia. 30–50 nm	Alumina tube	87
WO_3	Hexagonal WO_3	10	200	[a]	[a]	[a]	Dia. 50–100 nm	[a]	88
	Au-doped WO_3 thin film	0.05	250	63	88	1080	Thi. ~600 nm	Al_2O_3 substrate	89
	Pd-doped WO_3 film	0.5	25	90	[a]	[a]	Thi. 20 μM	Alumina substrate	91
In_2O_3	In_2O_3 rectangular nanoparticle	50	268.5	99	2	7	Dia. 50–80 nm	Alumina tube	120
	V-doped In_2O_3 nanofiber	13.9–50	90	~93	15	18	Dia. 95 nm	Ceramic tube	95
	Co-doped In_2O_3 nanoparticle	50	125	82	7	~300	Dia. 25 nm	Alumna tube	121
NiO	Fe_2O_3-loaded NiO nanoplate	10	200	~86	13–27	[a]	Thi. <500 nm	[a]	101
Homo- or hetero-heterojunction	CuO-loaded In_2O_3 nanofiber	5	150	~100	[a]	<140	Dia. ~10.2 ± 0.1 nm	Alumina substrate	109
	NiO decorated SnO_2 nanowire	10	300	~100	<20	102	[a]	Alumina substrate	111
	CuO-doped SnO_2 thin film	50	80–90	~100	<60	<50	[a]	Silicon substrate	122
	CuO–NiO core–shell microsphere	100	260	~98	18	29	Dia. 800 nm	[a]	113
Metal salt	$Fe_2(MoO_4)_3$ nanorod	5	80	~82	<30	<150	Dia. 200 nm, len. 1.2–4 μm	[a]	117
	β-$AgVO_3$ nanowire	50	250	[a]	<20	<10	Dia. 100–700 nm, len. 1–100 μM	[a]	118

[a] No reported or uncertain results. Dia., len., and thi. indicated the diameter, length, and thick of the nanomaterial.

Conflict of interest

The authors declare no competing financial interest.

Acknowledgements

This study was financially supported by the National Natural Science Foundation of China (51178171, 51378190, 51179068), the Program for Changjiang Scholars and Innovative Research Team in University (IRT-13R17).

Reference

1 X. Zhang, Y. Tang, S. Qu, J. Da and Z. Hao, *ACS Catal.*, 2015, **5**, 1053–1067.
2 Z. Li, Y. Xiao, W. Xue, Q. Yang and C. Zhong, *J. Phys. Chem. C*, 2015, **119**, 3674–3683.
3 J. Zhang, B. Dubey and T. Townsend, *Environ. Sci. Technol.*, 2014, **48**, 11777–11786.
4 K. Guo, J. Wen, Y. Zhao, Y. Wang, Z. Zhang, Z. Li and Z. Qian, *Environ. Sci. Technol.*, 2014, **48**, 6844–6849.
5 A. L. Ling, C. E. Robertson, J. K. Harris, D. N. Frank, C. V. Kotter, M. J. Stevens, N. R. Pace and M. T. Hernandez, *Environ. Sci. Technol.*, 2014, **48**, 7357–7364.
6 L. Li, L. Hu, Q. Zhou, C. Huang, Y. Wang, C. Sun and G. Jiang, *Environ. Sci. Technol.*, 2015, **49**, 2486–2495.
7 A. H. Nielsen, J. Vollertsen, H. S. Jensen, H. I. Madsen and T. Hvitved-Jacobsen, *Water Environ. Res.*, 2008, **80**, 16–25.
8 Z. Guo, G. Chen, G. Zeng, Z. Li, A. Chen, J. Wang and L. Jiang, *Analyst*, 2015, **140**, 1772–1786.
9 S. Singha, D. Kim, H. Moon, T. Wang, K. H. Kim, Y. H. Shin, J. Jung, E. Seo, S. J. Lee and K. H. Ahn, *Anal. Chem.*, 2015, **87**, 1188–1195.
10 Z. Dai, L. Tian, B. Song, Z. Ye, X. Liu and J. Yuan, *Anal. Chem.*, 2014, **86**, 11883–11889.
11 N. Adarsh, M. S. Krishnan and D. Ramaiah, *Anal. Chem.*, 2014, **86**, 9335–9342.
12 J. Hao, B. Xiong, X. D. Cheng, Y. He and E. S. Yeung, *Anal. Chem.*, 2014, **86**, 4663–4667.
13 Y. Y. Zhang, H. Zhou, P. Wu, H. R. Zhang, J. J. Xu and H. Y. Chen, *Anal. Chem.*, 2014, **86**, 8657–8664.
14 K. Drønen, I. Roalkvam, J. Beeder, T. Torsvik, I. H. Steen, A. Skauge and T. Liengen, *Environ. Sci. Technol.*, 2014, **48**, 8627–8635.
15 B. D. Gibson, R. T. Amos and D. W. Blowes, *Environ. Sci. Technol.*, 2011, **45**, 2863–2870.
16 M. Natter, J. Keevan, Y. Wang, A. R. Keimowitz, B. C. Okeke, A. Son and M. K. Lee, *Environ. Sci. Technol.*, 2012, **46**, 5744–5755.
17 S. Singkammo, A. Wisitsoraat, C. Sriprachuabwong, A. Tuantranont, S. Phanichphant and C. Liewhiran, *ACS Appl. Mater. Interfaces*, 2015, **7**, 3077–3092.
18 K. Suematsu, Y. Shin, Z. Hua, K. Yoshida, M. Yuasa, T. Kida and K. Shimanoe, *ACS Appl. Mater. Interfaces*, 2014, **6**, 5319–5326.
19 S. Jana and A. Mondal, *ACS Appl. Mater. Interfaces*, 2014, **6**, 15832–15840.
20 J. Huang, Y. Zhu, H. Zhong, X. Yang and C. Li, *ACS Appl. Mater. Interfaces*, 2014, **6**, 7055–7062.
21 G. Zhu, H. Xu, Y. Xiao, Y. Liu, A. Yuan and X. Shen, *ACS Appl. Mater. Interfaces*, 2012, **4**, 744–751.
22 F. Fan, Y. Feng, P. Tang, A. Chen, R. Luo and D. Li, *Ind. Eng. Chem. Res.*, 2014, **53**, 12737–12743.
23 T. S. Wang, Q. S. Wang, C. L. Zhu, Q. Y. Ouyang, L. H. Qi, C. Y. Li, G. Xiao, P. Gao and Y. J. Chen, *Sens. Actuators, B*, 2012, **171–172**, 256–262.
24 Y. Zhang, Q. Xiang, J. Q. Xu, P. C. Xu, Q. Y. Pan and F. Li, *J. Mater. Chem.*, 2009, **19**, 4701–4706.
25 Q. Y. Ouyang, L. Li, Q. S. Wang, Y. Zhang, T. S. Wang, F. N. Meng, Y. J. Chen and P. Gao, *Sens. Actuators, B*, 2012, **169**, 17–25.
26 Y. J. Chen, G. Xiao, T. S. Wang, F. Zhang, Y. Ma, P. Gao, C. L. Zhu, E. D. Zhang, Z. Xu and Q. H. Li, *Sens. Actuators, B*, 2011, **155**, 270–277.
27 X. Y. Xue, L. L. Xing, Y. J. Chen, S. L. Shi, Y. G. Wang and T. H. Wang, *J. Phys. Chem. C*, 2008, **112**, 12157–12160.
28 Y. Yan, H. Yu, Y. Zhang, K. Zhang, H. Zhu, T. Yu, H. Jiang and S. Wang, *ACS Appl. Mater. Interfaces*, 2015, **7**, 3547–3553.
29 B. Xiong, L. Peng, X. Cao, Y. He and E. S. Yeung, *Analyst*, 2015, **140**, 1763–1771.
30 C. Wei, Q. Zhu, W. Liu, W. Chen, Z. Xi and L. Yi, *Org. Biomol. Chem.*, 2014, **12**, 479–485.
31 W. Xuan, C. Sheng, Y. Cao, W. He and W. Wang, *Angew. Chem., Int. Ed.*, 2012, **51**, 2282–2284.
32 A. R. J. Lippert, *Inorg. Biochem.*, 2014, **133**, 136–142.
33 X. Fu, J. Liu, Y. Wan, X. Zhang, F. Meng and J. Liu, *J. Mater. Chem.*, 2012, **22**, 17782–17791.
34 S. K. Das, C. S. Lim, S. Y. Yang, J. H. Han and B. R. Cho, *Chem. Commun.*, 2012, **48**, 8395–8397.
35 W. M. Xuan, R. Pan, Y. T. Cao, K. J. Liu and W. Wang, *Chem. Commun.*, 2012, **48**, 10669–10671.
36 L. Li, J. Ge, H. Wu, Q. H. Xu and S. Q. Yao, *J. Am. Chem. Soc.*, 2012, **134**, 12157–12167.
37 A. Poser, C. Vogt, K. Knöller, J. Ahlheim, H. Weiss, S. Kleinsteuber and H. H. Richnow, *Environ. Sci. Technol.*, 2014, **48**, 9094–9102.
38 D. Goevert and R. Conrad, *Environ. Sci. Technol.*, 2008, **42**, 7813–7817.
39 A. D. Wiheeb, I. K. Shamsudin, M. A. Ahmad, M. N. Murat, J. Kim and M. R. Othman, *Rev. Chem. Eng.*, 2013, **29**, 449–470.
40 k. Sasakura, K. Hanaoka, N. Shibuya, Y. Mikami, Y. Kimura, T. Komatsu, T. Ueno, T. Terai, H. Kimura and T. Nagano, *J. Am. Chem. Soc.*, 2011, **133**, 18003–18005.
41 M. Y. Jia, L. Y. Niu, Y. Zhang, Q. Z. Yang, C. H. Tung, Y. F. Guan and L. Feng, *ACS Appl. Mater. Interfaces*, 2015, **7**, 5907–5914.
42 Y. Yang, J. M. Mathieu, S. Chattopadhyay, J. T. Miller, T. Wu, T. Shibata, W. Guo and P. J. J. Alvarez, *ACS Nano*, 2012, **6**, 6091–6098.

43 C. Levard, E. M. Hotze, G. V. Lowry and G. E. Brown Jr, *Environ. Sci. Technol.*, 2012, **46**, 6900–6914.
44 J. J. Chen, K. Wang, L. Hartman and W. L. Zhou, *J. Phys. Chem. C*, 2008, **112**, 16017–16021.
45 Q. Dong, Y. Shi, K. Wang, Y. Li, S. Wang, H. Zhang, Y. Xing, Y. Du, X. Bai and T. Ma, *J. Phys. Chem. C*, 2015, **119**, 10212–10217.
46 K. T. Lee, C. H. Lin and S. Y. Lu, *J. Phys. Chem. C*, 2014, **118**, 14457–14463.
47 H. Wang and A. L. Rogach, *Chem. Mater.*, 2014, **26**, 123–133.
48 J. Ding, X. Yan, J. Li, B. Shen, J. Yang, J. Chen and Q. Xue, *ACS Appl. Mater. Interfaces*, 2011, **3**, 4299–4305.
49 P. C. Hsu, C. J. Hsu, C. H. Chang, S. P. Tsai, W. C. Chen, H. H. Hsieh and C. C. Wu, *ACS Appl. Mater. Interfaces*, 2014, **6**, 13724–13729.
50 J. J. Lee, J. Y. Ha, W. K. Choi, Y. S. Cho and J. W. Choi, *ACS Comb. Sci.*, 2015, **17**, 247–252.
51 G. Martínez-Criado, J. Segura-Ruiz, M. H. Chu, R. Tucoulou, I. López, E. Nogales, B. Mendez and J. Piqueras, *Nano Lett.*, 2014, **14**, 5479–5487.
52 A. Nie, L. Y. Gan, Y. Cheng, H. Asayesh-Ardakani, Q. Li, C. ong, R. Tao, F. Mashayek, H. T. Wang, U. Schwingenschlö gl, R. F. Klie and R. S. Yassar, *ACS Nano*, 2013, **7**, 6203–6211.
53 Y. C. Her, B. Y. Yeh and S. L. Huang, *ACS Appl. Mater. Interfaces*, 2014, **6**, 9150–9159.
54 S. W. Choi, A. Katoch, G. J. Sun, J. H. Kim, S. H. Kim and S. S. Kim, *ACS Appl. Mater. Interfaces*, 2014, **6**, 8281–8287.
55 R. Müller, F. Hernandez-Ramirez, H. Shen, H. Du, W. Mader and S. Mathur, *Chem. Mater.*, 2012, **24**, 4028–4035.
56 J. Pan, R. Ganesan, H. Shen and S. Mathur, *J. Phys. Chem. C*, 2010, **114**, 8245–8250.
57 J. Pan, J. Zhang, H. Shen, Q. Xiong and S. Mathur, *J. Phys. Chem. C*, 2012, **116**, 13835–13836.
58 A. Shaposhnik, S. Ryabtsev, F. Shao, F. Hernandez-Ramirez, J. Morante, A. Zviagin, N. Meshkova, D. Shaposhnik and A. Vasiliev, *Procedia Eng.*, 2012, **47**, 1398–1401.
59 T. Minami, *J. Sol-Gel Sci. Technol.*, 2013, 4–11.
60 N. Ma, K. Suematsu, M. Yuasa, T. Kida and K. Shimanoe, *ACS Appl. Mater. Interfaces*, 2015, **7**, 5863–5869.
61 S. Law, L. Yu, A. Rosenberg and D. Wasserman, *Nano Lett.*, 2013, **13**, 4569–4574.
62 S. M. Zhang, P. P. Zhang, Y. Wang, Y. Y. Ma, J. Zhong and X. H. Sun, *ACS Appl. Mater. Interfaces*, 2014, **6**, 14975–14980.
63 A. W. Tang, S. C. Qu, K. Li, Y. B. Hou, F. Teng, J. Cao, Y. S. Wang and Z. G. Wang, *Nanotechnology*, 2010, **21**, 285602.
64 W. Wei, Y. Dai and B. B. Huang, *J. Phys. Chem. C*, 2011, **115**, 18597–18602.
65 M. V. Vaishampayan, R. G. Deshmukh, P. Walke and I. S. Mulla, *Mater. Chem. Phys.*, 2008, **109**, 230–234.
66 C. J. Jin, T. Yamazaki, K. Ito, T. Kikuta and N. Nak, *Vacuum*, 2006, **80**, 723–725.
67 K. J. Iversen and M. J. S. Spencer, *J. Phys. Chem. C*, 2013, **117**, 26106–26118.
68 C. M. Ghimbeu, J. Schoonman, M. Lumbreras and M. Siadat, *Appl. Surf. Sci.*, 2007, **253**, 7483–7489.
69 J. Kim and K. Yong, *J. Phys. Chem. C*, 2011, **115**, 7218–7224.
70 C. H. Wang, X. F. Chu and M. M. Wu, *Sens. Actuators, B*, 2006, **113**, 320–323.
71 Y. L. Cao, D. Z. Jia, R. Y. Wang and J. M. Luo, *Solid-State Electron.*, 2013, **82**, 67–71.
72 P. K. Sharma, N. S. Ramgir, C. P. Goyal, N. Dattl, S. Srivastava, M. Kaul, A. K. Debnath, D. K. Aswal, Y. K. Vijay and S. K. Gupta. *Proceedings of the "International Conference on Advanced Nanomaterials & Emerging Engineering Technologies"*. 2013, pp. 215–217.
73 N. V. Long, Y. Yang, M. Yuasa, C. M. Thi, Y. Cao, T. Nann and M. Nogami, *RSC Adv.*, 2014, **4**, 8250–8255.
74 D. Peeters, D. Barreca, G. Carraro, E. Comini, A. Gasparotto, C. Maccato, C. Sada and G. Sberveglieri, *J. Phys. Chem. C*, 2014, **118**, 11813–11819.
75 Y. Wang, S. Wang, H. Zhang, X. Gao, J. Yang and L. Wang, *J. Mater. Chem. A*, 2014, **2**, 7935–7943.
76 C. Wang, X. Cheng, X. Zhou, P. Sun, X. Hu, K. Shimanoe, G. Lu and N. Yamazoe, *ACS Appl. Mater. Interfaces*, 2014, **6**, 12031–12037.
77 X. Li, W. Wei, S. Wang, L. Kuai and B. Geng, *Nanoscale*, 2011, **3**, 718–724.
78 Q. Hao, L. Li, X. Yin, S. Liu, Q. Li and T. Wang, *Mater. Sci. Eng., B*, 2011, **176**, 600–605.
79 V. Balouria, A. Kumar, S. Samanta, A. Singh, A. K. Debnath, A. Mahajan, R. K. Bedi, D. K. Aswal and S. K. Gupta, *Sens. Actuators, B*, 2013, **181**, 471–478.
80 C. Gleitzer, *Key Eng. Mater.*, 1996, **125–126**, 355–418.
81 J. M. Ma, J. Zhang, S. R. Wang, T. H. Wang, J. B. Lian, X. C. Duan and W. J. Zheng, *J. Phys. Chem. C*, 2011, **115**, 18157–18163.
82 J. M. Ma, J. Zhang, S. R. Wang, Q. H. Wang, L. F. Jiao, J. Q. Yang, X. C. Duan, Z. F. Liu, J. B. Lian and W. J. Zheng, *CrystEngComm*, 2011, **13**, 6077–6081.
83 J. Ma, L. Mei, Y. Chen, Q. Li, T. Wang, Z. Xu, X. Duan and W. Zheng, *Nanoscale*, 2013, **5**, 895–898.
84 J. Deng, J. Ma, L. Mei, Y. Tang, Y. Chen, T. Lv, Z. Xu and T. Wang, *J. Mater. Chem. A*, 2013, **1**, 12400–12403.
85 Y. Wang, F. Kong, B. Zhu, S. Wang, S. Wu and W. Huang, *Mater. Sci. Eng., B*, 2007, **140**, 98–102.
86 Y. Wang, S. Wang, Y. Zhao, B. hu, F. Kong, D. Wang, S. Wu, W. Huang and S. Zhang, *Sens. Actuators, B*, 2007, **125**, 79–84.
87 Y. Wang, Y. Wang, J. Cao, F. Kong, H. Xia, J. Zhang, B. Zhu, S. Wang and S. Wu, *Sens. Actuators, B*, 2008, **131**, 183–189.
88 I. M. Szilá gyi, S. Saukko, J. Mizsei, A. L. Tóth, J. Madarász and G. Pokol, *Solid State Sci.*, 2010, **12**, 1857–1860.
89 N. Datta, N. Ramgir, M. Kaur, M. Roy, R. Bhatt, S. Kailasaganapathi, A. K. Debnath, D. K. Aswal and S. K. Gupta, *Mater. Chem. Phys.*, 2012, **134**, 851–857.
90 J. Gabrusenoks, A. Veispals, A. von Czarnowski and K. H. Meiwes-Broer, *Electrochim. Acta*, 2001, **46**, 2229–2231.
91 A. Hoel, L. F. Reyes, S. Saukko, P. Heszler, V. Lantto and C. G. Granqvist, *Sens. Actuators, B*, 2005, **105**, 283–289.
92 C. Feng, X. Li, J. Ma, Y. Sun, C. Wang, P. Sun, J. Zheng and G. Lu, *Sens. Actuators, B*, 2015, **209**, 622–629.

93 C. Zhao, B. Huang, E. Xie, J. Zhou and Z. Zhang, *Sens. Actuators, B*, 2015, **207**, 313–320.
94 L. Gao, Z. Cheng, Q. Xiang, Y. Zhang and J. Xu, *Sens. Actuators, B*, 2015, **208**, 436–443.
95 J. Liu, W. Guo, F. Qu, C. Feng, C. Li, L. Zhu, J. Zhou, S. Ruan and W. Chen, *Ceram. Int.*, 2014, **40**, 6685–6689.
96 N. Ahmadaghaei and M. Noei, *J. Iran. Chem. Soc.*, 2014, **11**, 725–731.
97 G. Zhu, C. Xi, H. Xu, D. Zheng, Y. Liu, X. Xu and X. Shen, *RSC Adv.*, 2012, **2**, 4236–4241.
98 C. Dong, X. Xiao, G. Chen, H. Guan, Y. Wang and L. Djerdj, *RSC Adv.*, 2015, **5**, 4880–4885.
99 P. Rai, J. W. Yoon, H. M. Jeong, S. J. Hwang, C. H. Kwak and J. H. Lee, *Nanoscale*, 2014, **6**, 8292–8299.
100 J. Zhang, D. Zeng, S. Zhao, J. Wu, K. Xu, Q. Zhu, G. Zhang and C. Xie, *Phys. Chem. Chem. Phys.*, 2015, **17**, 14903–14911.
101 F. Li, Y. Chen and J. Ma, *RSC Adv.*, 2014, **4**, 14201–14205.
102 G. J. Sun, S. W. Choi, A. Katoch, P. Wu and S. S. Kim, *J. Mater. Chem. C*, 2013, **1**, 5454–5462.
103 L. Wang, J. Deng, Z. Lou and T. Zhang, *J. Mater. Chem. A*, 2014, **2**, 10022–10028.
104 T. Jiang, Z. Wang, Z. Li, W. Wang, X. Xu, X. Liu, J. Wang and C. Wang, *J. Mater. Chem. C*, 2013, **1**, 3017–3025.
105 H. Ohta, M. Hirano, K. Nakahara, H. Maruta, T. Tanabe, M. Kamiya, T. Kamiya and H. Hosono, *Appl. Phys. Lett.*, 2003, **5**, 1029–1031.
106 Z. J. Wang, Z. Y. Li, J. H. Sun, H. N. Zhang, W. Wang, W. Zheng and C. Wang, *J. Phys. Chem. C*, 2010, **114**, 6100–6105.
107 J. Kim, W. Kim and K. Yong, *J. Phys. Chem. C*, 2012, **116**, 15682–15691.
108 S. J. Kim, C. W. Na, I. S. Hwang and J. H. Lee, *Sens. Actuators, B*, 2012, **168**, 83–89.
109 X. Liang, T. H. Kim, J. W. Yoon, C. H. Kwak and J. H. Lee, *Sens. Actuators, B*, 2015, **209**, 934–942.
110 L. Xu, R. Zheng, S. Liu, J. Song, J. Chen, B. Dong and H. Song, *Inorg. Chem.*, 2012, **51**, 7733–7740.
111 N. V. Hieu, P. T. H. Van, L. T. Nhan, N. V. Duy and N. D. Hoa, *Appl. Phys. Lett.*, 2012, **101**, 253106.
112 E. D. Gaspera, M. Guglielmi, S. Agnoli, G. Granozzi, M. L. Post, V. Bello, G. Mattei and A. Martucci, *Chem. Mater.*, 2010, **22**, 3407–3417.
113 Y. Wang, F. Qu, J. Liu, Y. Wang, J. Zhou and S. Ruan, *Sens. Actuators, B*, 2015, **209**, 515–523.
114 A. B. Bodade, A. M. Bende and G. N. Chaudhari, *Vacuum*, 2008, **82**, 588–593.
115 J. E. Gatt, H. Nair and C. D. Baertsch, *Appl. Catal., B*, 2010, **99**, 127–134.
116 J. Tuček, K. C. Kemp, K. S. Kim and R. Zbořil, *ACS Nano*, 2014, **8**, 7571–7612.
117 Y. J. Chen, X. M. Gao, X. P. Di, Q. Y. Ouyang, P. Gao, L. H. Qi, C. Y. Li and C. L. Zhu, *ACS Appl. Mater. Interfaces*, 2013, **5**, 3267–3274.
118 L. Mai, L. Xu, Q. Gao, C. Han, B. Hu and Y. Pi, *Nano Lett.*, 2010, **10**, 2604–2608.
119 E. Bruneta, T. Maiera, G. C. Mutinatia, S. Steinhauera, A. Köcka, C. Gspanb and W. Groggerb, *Sens. Actuators, B*, 2012, **165**, 110–118.
120 J. Xu, X. Wang and J. Shen, *Sens. Actuators, B*, 2006, **115**, 642–646.
121 V. D. Kapse, S. A. Ghosh, G. N. Chaudhari and F. C. Raghuwanshi, *Talanta*, 2008, **76**, 610–616.
122 Y. D. Wu, M. S. Tong, X. L. He, Y. S. Zhang and G. R. Dai, *Sens. Actuators, B*, 2001, **79**, 187–191.